

# Electronic correlations in vanadium chalcogenides: BaVSe<sub>3</sub> vs. BaVS<sub>3</sub>

Daniel Grieger, Lewin Boehnke and Frank Lechermann

I. Institut für Theoretische Physik, Universität Hamburg, Jungiusstr. 9,  
D-20355 Hamburg, Germany

E-mail: daniel.grieger@physnet.uni-hamburg.de

**Abstract.** Albeit structurally and electronically very similar, at low temperature the quasi-onedimensional vanadium sulfide BaVS<sub>3</sub> shows a metal-to-insulator transition via the appearance of a charge-density-wave state, while BaVSe<sub>3</sub> apparently remains metallic down to zero temperature. This different behavior upon cooling is studied by means of density functional theory and its combination with the dynamical mean-field theory and the rotationally-invariant slave-boson method. We reveal several subtle differences between these chalcogenides that provide indications for the deviant behavior of BaVSe<sub>3</sub> at low temperature. In this regard, a smaller Hubbard  $U$  in line with an increased relevance of the Hund's exchange  $J$  plays a vital role.

PACS numbers: 71.30.+h, 71.15.Mb, 71.10.Fd

Submitted to: *J. Phys.: Condens. Matter*

## 1. Introduction

The discussion of electronic correlation effects in  $3d$ -transition-metal compounds appears often dominantly reserved for the physics of oxides, e.g. for cuprates, manganites, ruthenates, or more recently, cobaltates. However there is increasing awareness that strong correlation effects are also relevant for many intriguing electronic phase transitions of various chalcogenides such as, e.g. the metal-insulator transition (MIT) in NiS<sub>2-x</sub>Se<sub>x</sub> [1], the charge-density wave (CDW) transition in NbSe<sub>3</sub> [2] or the recent discovery of higher-temperature superconductivity in Fe-chalcogenides. In this respect, the vanadium chalcogenides with the quasi-twodimensional X-VS<sub>2</sub> misfit-layer structures [3] and the quasi-onedimensional (1D) BaV(S,Se)<sub>3</sub> systems offer a unique opportunity to study the interplay of correlation effects and effective low-dimensionality in these transition-metal compound systems.

Here we want to concentrate on the subtle comparison of the quasi-1D barium vanadium chalcogenide systems. It will become evident that the vanadium selenide BaVSe<sub>3</sub> is in effect rather similar to the corresponding vanadium sulfide BaVS<sub>3</sub> in many respects. The latter compound has been subject to various studies concerning

its complex electronic structure throughout the last decades [4, 5, 6, 7, 8, 9, 10, 11, 12]. This sulfide exhibits three continuous phase transitions with decreasing temperature, one of which is a highlighting metal-to-paramagnetic-insulator transition at  $T_{MIT} \sim 70K$ . Though the very details on the scenario are still to be revealed, strong evidence exists [13, 11] that this transition is associated with a CDW instability. Interestingly, such a transition cannot be found in the similar selenide compound, which remains metallic down to very low temperatures [14]. This raises questions about the delicate electronic and structural differences that anticipate a possible CDW in these chalcogenides. Hence the present investigation is devoted to a detailed comparison between the correlated electronic structure of  $BaVS_3$  and  $BaVSe_3$ .

Concerning the structural properties, many features of  $BaVSe_3$  are akin to the ones of  $BaVS_3$ . At room temperature, both materials exhibit a hexagonal structure in which the vanadium atoms form straight chains in the crystallographic  $c$  direction. The intrachain V-V distance is less than half of the interchain distance, so that one is tempted to identify a quasi-(1D) substructure in these compounds. The chains become slightly distorted in the  $ab$  plane with a zigzag distortion in the  $bc$  plane at the continuous transition temperature  $T_S \sim (240K, 290K)$  (sulfide, selenide) [15, 16]. Thus below this temperature regime, an orthorhombic crystal structure is stabilized for both materials. Furthermore, the additional metal-to-insulator transition of the sulfide is accompanied by a doubling of the unit cell and a transition to the monoclinic crystal system [13], whereas the selenide remains orthorhombic down to very low temperature. Both chalcogenides display local-moment behavior at ambient  $T$  and a final continuous magnetic ordering transition. While in  $BaVS_3$  an incommensurate antiferromagnetic order develops below  $T_X \sim 30K$  [17],  $BaVSe_3$  undergoes a ferromagnetic transition at  $T_C \sim 43K$  [16, 18].

The electronic structure of both materials in the low-energy regime is dominated by the nominal  $V^{4+}$  valence, so that they can be described as  $3d^1$  compounds with a  $t_{2g}$ -like manifold at the Fermi level [5, 10, 12]. The latter consists of an  $A_{1g}$ -like orbital pointing along the vanadium chain direction as well as two  $E_g$ -like orbitals pointing inbetween the neighboring sulfur/selenium ions, respectively. Due to strong hybridization with  $S(3p)/Se(4p)$ , the  $V(e_g)$  states have mainly high-energy weight and may be integrated out in a first low-energy approximation. Hence the essential physics of these systems can be described within a three-band model approach [12]. The two  $E_g$  states are degenerate in the hexagonal structure, but split into an  $E_{g1}$  and an  $E_{g2}$  state in the orthorhombic regime. Due to their somewhat isolated orbital space, the hybridization with the environment is comparably small. For this reason, they form very narrow bands that show almost no dispersion. In contrary, the  $A_{1g}$  orbitals display a larger dispersion along the V chain direction. Hence in a minimal model, the physics of these materials essentially boils down to the interplay of an itinerant and two localized states sharing a single electron.

## 2. Theoretical Framework

Due to the obviously delicate electronic systems in  $BaVS_3$  and  $BaVSe_3$  with narrow bands at the Fermi level and local-moment physics, methods are needed that allow to take into account many-body effects explicitly, i.e., beyond standard density functional theory (DFT) in its local density approximation (LDA) to the exchange-correlation energy. In the present work, the opportunity is taken to compare two different approaches for this task, namely the LDA+DMFT [19, 20] framework in conjunction with a highly-evolved quantum-Monte-Carlo impurity solver as well as the combination of LDA with the rotationally-invariant slave-boson formalism (RISB) [21, 22].

The DFT parts of the following calculations have been performed using a mixed-basis pseudopotential (MBPP) code [23], which utilizes norm-conserving pseudopotentials and a combined basis set of plane waves as well as non-overlapping localized functions. From the LDA band structure, by means of the maximally-localized Wannier function construction [24, 25, 26], a low-energy Kohn-Sham (KS) hamiltonian  $H_{\text{KS}}^{(C)}(\mathbf{k})$  within a correlated subspace  $\mathcal{C}$  is extracted [27]. In this work we restrict all self-energy effects to that subspace and hence may write the local interacting Green's function as

$$G_{mm'}(i\omega_n) = \sum_{\mathbf{k}} \left\{ [(i\omega_n + \mu)\mathbb{1} - H_{\text{KS}}^{(C)}(\mathbf{k}) - \Sigma^{(C)}(i\omega_n)]^{-1} \right\}_{mm'}. \quad (1)$$

Here  $\omega_n$  are Matsubara frequencies and  $\Sigma^{(C)}$  is the self-energy matrix for the correlated orbitals denoted by  $m, m'$ . Note that (1) is written in the DMFT approximation, i.e., with a purely local self-energy (for a review see e.g. [28]). The mean-field version of the RISB which is put into practise in the present work also has a local self-energy by construction. Moreover, the RISB self-energy only captures the linear term of the frequency dependence, expressed via the quasiparticle weight  $Z$ , as well as a local static part [12]. Thus without going into details, the main differences between DMFT and RISB (in mean-field version) is the neglect of the frequency dependence of the higher-energy excitations in the latter framework. However as a saddle-point approximation the performance is rather efficient with reliable qualitative (and often even good quantitative) results in most cases. It is also important to realize that although we use here a lattice-implementation of the RISB method, this technique may equally well be utilized as an impurity solver for standard DMFT. Due to the inherent local nature at saddle-point, this specific DMFT impurity solution is then identical to the direct lattice-calculation result.

In the present work, the explicit quantum impurity problem within DMFT is solved using the continuous-time quantum-Monte-Carlo (CTQMC) approach employing the hybridization-expansion method [29]. For the actual computations the recent implementation by Parcollet *et al.* (see also [30]) is employed. Both frameworks, i.e., DMFT(CTQMC) and RISB, allow for non-density-density terms in the many-body hamiltonian, which we restrict in the present case to spin-flip and pair-hopping processes.

Thus the following interacting hamiltonian for the minimal modeling may be used:

$$\begin{aligned} \hat{H}_{\text{int}} = & U \sum_m \hat{n}_{m\uparrow} \hat{n}_{m\downarrow} + \frac{1}{2} \sum_{m \neq m'} \sum_{\sigma} [U' \hat{n}_{m\sigma} \hat{n}_{m'\bar{\sigma}} + (U' - J) \hat{n}_{m\sigma} \hat{n}_{m'\sigma}] \\ & + \frac{1}{2} \sum_{m \neq m'} \sum_{\sigma} [J \hat{d}_{m\sigma}^{\dagger} \hat{d}_{m'\bar{\sigma}}^{\dagger} \hat{d}_{m\bar{\sigma}} \hat{d}_{m'\sigma} + J_C \hat{d}_{m\sigma}^{\dagger} \hat{d}_{m\bar{\sigma}}^{\dagger} \hat{d}_{m'\bar{\sigma}} \hat{d}_{m'\sigma}] \quad , \end{aligned} \quad (2)$$

where  $n_{m\sigma} = d_{m\sigma}^{\dagger} d_{m\sigma}$ , with  $d_{m\sigma}^{(\dagger)}$  as the electron annihilation (creation) operator for orbital  $m$  and spin  $\sigma$ . Throughout the calculations, the choice  $U' = U - 2J$  and  $J_C = J$ , appropriate for  $t_{2g}$  systems, is made.

### 3. Results

#### 3.1. LDA studies

The following LDA comparison between  $BaVS_3$  and  $BaVSe_3$  builds up on the orthorhombic crystal structure (space group  $Cmc2_1$ ), since we are mainly interested in elucidating the possibility of the CDW state in both systems. Note that the CDW instability is not only absent in the selenide compound, but vanishes also in the sulfide at high pressure [9]. This raised the suspicion that the selenide compound may be interpreted as the high-pressure analogue of the sulfide compound [14]. In any case, theoretically investigating  $BaVSe_3$  should surely also provide more information about the origin of the apparent CDW instability in  $BaVS_3$ .

The existence of the orthorhombic phase of the selenide has been reported already on the occasion of its first synthesis by Kelber *et al.* [16], but to the authors' knowledge no detailed experimental structural data is available in literature. For this reason, the atomic positions used for  $Cmc2_1$ - $BaVSe_3$  are revealed by structural relaxation within LDA using the MBPP code, while the crystal parameters are based on similar recent calculations performed by Akrap *et al.* [14]. In contrast, structural data obtained by neutron diffraction by Ghedira *et al.* [31] is used for  $BaVS_3$ . The crystal parameters ( $a, b, c$ ) for one unit cell consisting of two formula units of  $BaVS_3$  or  $BaVSe_3$ , respectively, in a.u. read (12.77, 21.71, 10.58) for  $BaVS_3$  and (13.34, 22.68, 11.06) for  $BaVSe_3$ . For both materials the ideal quasi-1D chains of vanadium ions are slightly distorted in the orthorhombic phase, leading to zig-zag chains. This effect turns out to be slightly larger in the selenide (relative displacement: 0.025) than in the sulfide (0.021). Concerning the electronic structure, figure 1 shows the LDA density of states (DOS) of  $BaVSe_3$  in a comparatively large energy window around the Fermi level. Analogous to  $BaVS_3$  [12], it can be seen that the low-energy physics of the material may be dominantly described by the above mentioned  $t_{2g}$  manifold. Thus a downfolding to an effective three-band model consisting of a broader  $A_{1g}$ -like level and narrower  $E_{g1}$ -like and  $E_{g2}$ -like levels is a suitable approximation for the essential physics. The accordance with the LDA DOS of the sulfide (shown in [12]) on this level of comparison is rather striking and only minor differences show up. Figure 2 compares the band structure of  $BaVSe_3$  and of  $BaVS_3$  in a smaller energy window, with 'fatbands' showing the weight of the symmetry-adapted

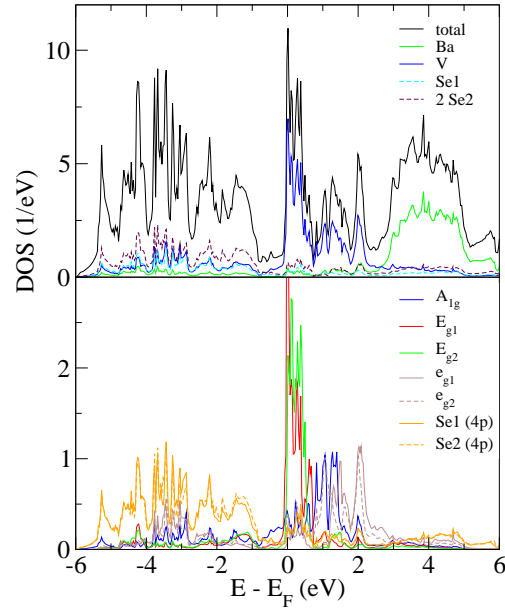


**Figure 1.** (Color online) LDA density of states of  $BaVSe_3$ .

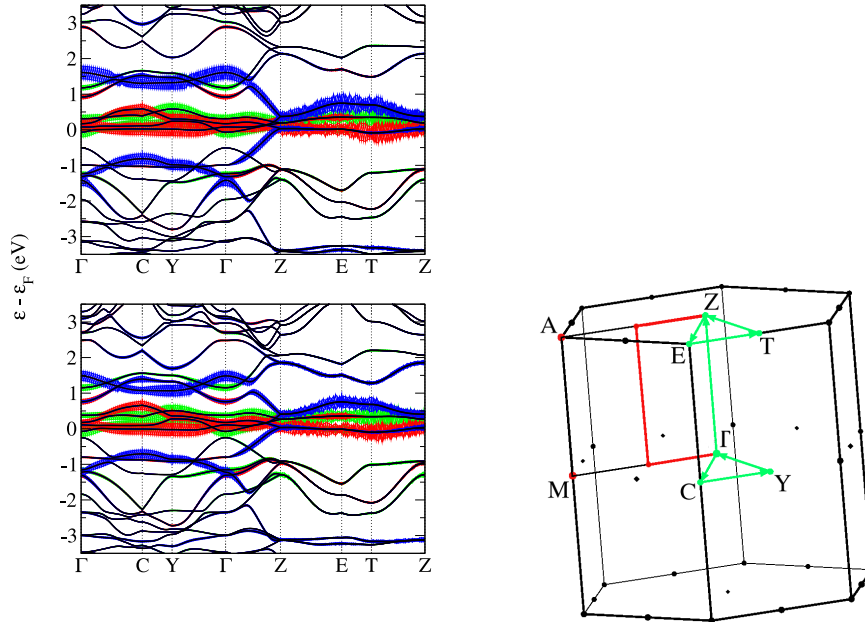


**Figure 2.** (Color online) Left: LDA band structure of  $BaVS_3$  (top) and  $BaVSe_3$  (bottom). The fatband broadening depicts the weight of  $t_{2g}$  orbitals on the bands. Color coding:  $A_{1g}$  (blue),  $E_{g1}$  (red) and  $E_{g2}$  (green). Right: Brillouin zone of the orthorhombic structure with relevant points/directions.

$t_{2g}$  states on the specific bands. Again both band structures are similar, yet subtle difference may be observed. First the Se(4p) band at the  $\Gamma$  point is much closer to the Fermi level than the corresponding S(3p) band in  $BaVS_3$ , which may lead to a smaller

Hubbard  $U$  for the minimal 3-band model due to increased screening. Furthermore the bandwidth difference between the three  $t_{2g}$  bands is reduced, i.e., the  $A_{1g}$ -like bands become narrower and the  $E_g$ -like ones broader. Hence the total  $t_{2g}$  bandwidth in  $BaVSe_3$  is slightly smaller ( $\sim 2.4$  eV) than in  $BaVS_3$  ( $\sim 2.7$  eV). This may be explained by the fact that since the larger Se ions give rise to increased interatomic distances, a smaller  $A_{1g}$ -like hopping amplitude along the chains results. As a general feature, the overall  $A_{1g}$  contribution to the bands seems somewhat more distributed in  $BaVSe_3$ . This enhanced spread in energy is again providing hints towards a larger degree of, eventually more isotropic, localization in the selenide.

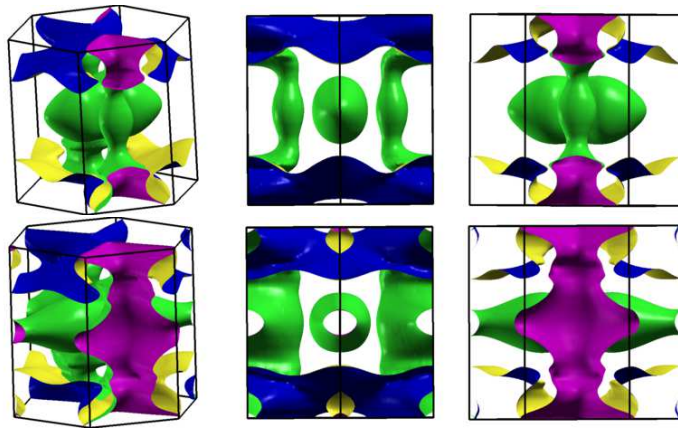


**Figure 3.** (Color online) LDA Fermi surfaces of  $BaVS_3$  (top) and  $BaVSe_3$  (bottom) from different perspectives.

Experimentally the nesting condition for the formation of the CDW was detected as  $2\mathbf{k}_F = 0.5\mathbf{c}^*$  [11], where  $\mathbf{c}^*$  is the reciprocal lattice vector along the  $c$  axis. In order to theoretically examine this condition, it is necessary to study the topology of the Fermi surface (FS) (see figure 3). Therefrom the nesting condition is not fulfilled in the pure LDA result in both materials. However somewhat surprisingly, the quasi-1D sheet of the selenide is closer to fulfill the experimental nesting condition than the corresponding sulfide sheet in LDA. On the opposite, the pillar-like structures are much more enhanced in the selenide. Hence differences in the  $t_{2g}$  occupations between the two compounds may be expected. Figure 4 shows the respective three-band dispersion of the correlated subspace obtained from a maximally-localized Wannier construction [24] for strongly hybridized bands [25]. It shall be mentioned that this construction yields for the selenide a larger spread of the Wannier functions (i.e., in the range of 23 a.u.<sup>2</sup> for the  $E_g$ -like ones in  $BaVSe_3$  compared to about 18 a.u.<sup>2</sup> for the same ones in  $BaVS_3$ ). This can be attributed to a stronger hybridization of the  $t_{2g}$  system with the Se( $4p$ ) electrons. Note that for the further use of this Wannier representation we rotated the original maximally-localized Wannier hamiltonian into the crystal-field basis, i.e., the basis where the on-site part thereof takes on a diagonal form.

Concerning the susceptibility towards the CDW state it is important and evident to note that the nesting vector mentioned above is not necessarily located along the  $\Gamma$ - $Z$

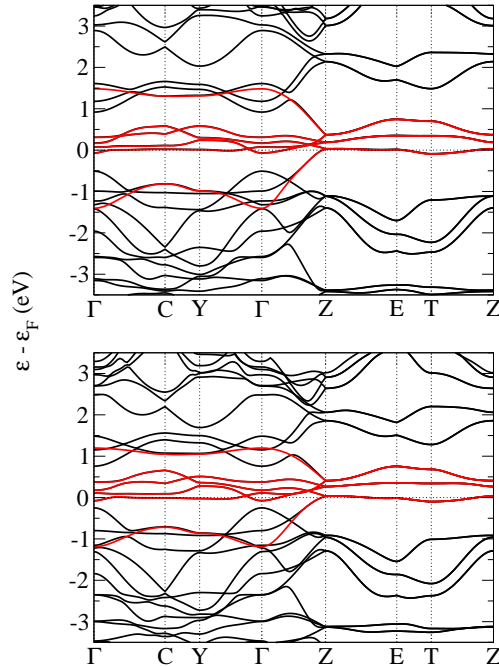


**Figure 4.** (Color online) Dispersions of the effective three-band model (red), obtained by means of a maximally-localized Wannier-function construction, for  $BaVS_3$  (top) and  $BaVSe_3$  (bottom). Black: original LDA band structure.

high-symmetry line [27, 12]. In order to take this fact into account, the low-energy band structure is computed along a Brillouin zone (BZ) path containing a line parallel to the  $\Gamma$ - $Z$  line, shown in figure 5. The points ' $M/2$ ' and ' $A/2$ ' are located halfway between the  $\Gamma$ - or  $Z$ -point, respectively, and the edge of the first BZ (see figure 2). From the displayed fatbands it can be seen that the hybridization between  $A_{1g}$  and  $E_{g1}$  on the resulting bands along  $M/2$ - $A/2$  as well as along  $\Gamma$ - $Z$  is significantly larger in the selenide than in the sulfide. Thus a clear notion of exclusive ' $A_{1g}$  bands' or ' $E_{g1}$  bands' becomes even more difficult for  $BaVSe_3$ . This fact impedes also the assignment of the distinct FS sheets to a single definite orbital character.

### 3.2. Inclusion of correlation effects

Besides the apparent metal-to-insulator transition in  $BaVS_3$ , already the complex magnetic behavior in both systems (with different magnetic order at low temperature) shows clearly the importance of electronic correlations in these vanadium chalcogenides. Hence a deeper comparison of  $BaVS_3$  and  $BaVSe_3$  has to include explicit many-body physics, which we approached with the LDA+DMFT(CTQMC) method as well as the LDA+RISB technique. This twofold investigation was elaborated in order to evaluate the reliability of the latter method compared to the more complete CTQMC impurity solution within DMFT. In the following, all the presented CTQMC impurity computations were performed at  $T=116K$  ( $\beta=100 \text{ eV}^{-1}$ ) and including spin-flip and pair-hopping terms in the interacting hamiltonian (if not stated differently).

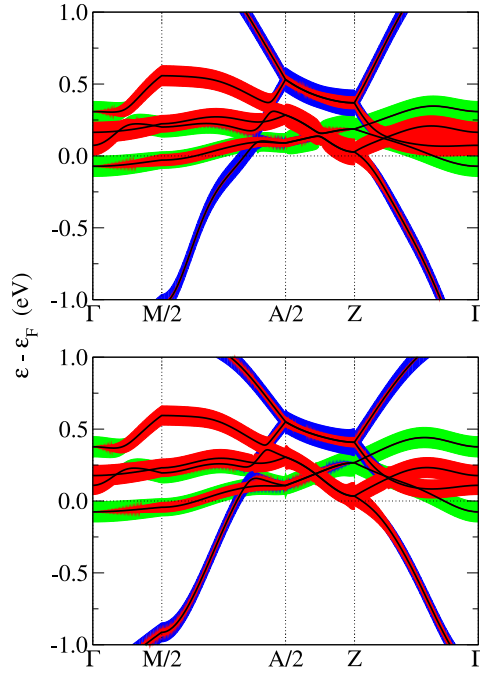


**Figure 5.** (Color online) LDA  $t_{2g}$  Wannier fatband plots for  $BaVS_3$  (top) and  $BaVSe_3$  (bottom) along a closed path in the first Brillouin zone, connecting  $\Gamma$ , 'M/2', 'A/2' and Z (see figure 2). Color coding:  $A_{1g}$  (blue),  $E_{g1}$  (red) and  $E_{g2}$  (green).

In [32], a chosen value of  $U=3.5$  eV lead to a proper theoretical description of

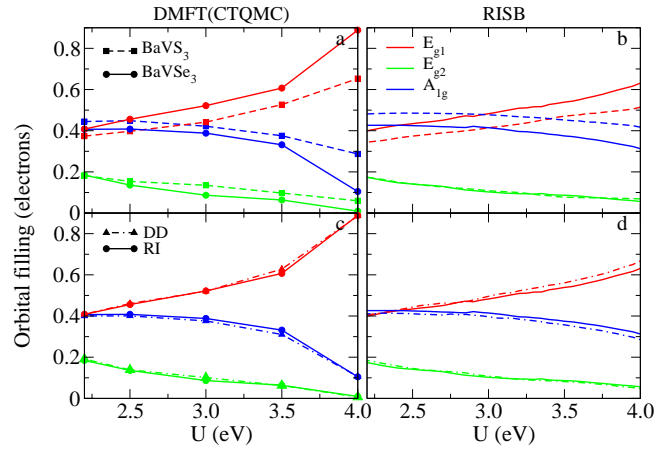


**Figure 6.** (Color online) (a-b): Effective  $t_{2g}$  fillings for  $BaVS_3$  (dashed/squares) and  $BaVSe_3$  (solid/circles) using the KS-Wannier hamiltonians with increasing  $U$ . (c-d): Fillings for  $BaVSe_3$  using only density-density terms (dash-dotted/triangles) and including spin-flip as well as pair-hopping terms (solid/circles). (a, c): CTQMC solution of DMFT and (b, d): RISB solution.

**Table 1.** Orbital-resolved fillings from LDA+DMFT(CTQMC). Vanishing Hubbard  $U$  marks the LDA result. 'DD': only density-density interactions, 'RI': additional inclusion of spin-flip and pair-hopping interactions.

	$U$ (eV)	$\hat{H}_{\text{int}}$	$A_{1g}$	$E_{g1}$	$E_{g2}$
BaVS <sub>3</sub>	0.0		0.58	0.31	0.11
	3.5	DD	0.38	0.54	0.08
	3.5	RI	0.37	0.53	0.10
BaVSe <sub>3</sub>	0.0		0.49	0.40	0.11
	2.5	DD	0.40	0.46	0.14
	2.5	RI	0.41	0.45	0.14
	3.5	DD	0.31	0.63	0.06
	3.5	RI	0.33	0.61	0.06

BaVS<sub>3</sub>. In this work we also do not compute the interaction parameters from first principles, but again take on a practical point of view in order to account for the key correlation effects. As noted in the previous section, the corresponding Hubbard  $U$  for BaVSe<sub>3</sub> is expected to be smaller because of the increased screening capabilities of the Se(4*p*) electrons compared to the S(3*p*) ones. In order to compare BaVS<sub>3</sub> and BaVSe<sub>3</sub> in this respect, the calculated orbital-resolved fillings are shown in figure 6 for varying values of  $U$  and fixed Hund's exchange  $J=0.7$  eV. First note the very good agreement between the DMFT(CTQMC) and the RISB treatment of the correlation effects. Both methods clearly show the correlation-induced charge transfer mainly between the  $A_{1g}$  and  $E_{g1}$  orbitals [32, 12]. The actual numbers surely differ somewhat between both approaches due to the neglect of the explicit quantum fluctuations within RISB, especially concerning the frequency dependence of the high-energy excitations. But also the trend in the (minor) differences between density-density only terms and the inclusion of more general terms in the interacting hamiltonian is still well reproduced by the simplified RISB technique. Concerning the physics, it is visible that the  $A_{1g}$  filling is generally reduced in the selenide compared to the sulfide, which was already expected from the Fermi-surface discussion. This result is also apparent from table 1, where the occupation numbers are displayed for selected interaction strengths. In this context, a smaller Hubbard interaction  $U=2.5$  eV for BaVSe<sub>3</sub> seems reasonable in the end. However for direct comparisons we also include the case  $U=3.5$  eV in the computations. Note that  $J$  is usually not strongly affected by the crystal environment and to a good approximation can remain constant. Hence if not stated differently, we generally fixed the Hund's coupling to a reasonable value of  $J=0.7$  eV. In summary, the system could be understood as an effective two-band system, since the effective  $E_{g2}$  orbital is almost empty, with an even larger correlation-induced charge transfer from  $A_{1g}$  to  $E_{g1}$  in the selenide than in the sulfide. It can further be seen that the spin-flip and pair-hopping terms have only a small influence on the occupation numbers, resulting qualitatively in a slightly smaller orbital polarization.

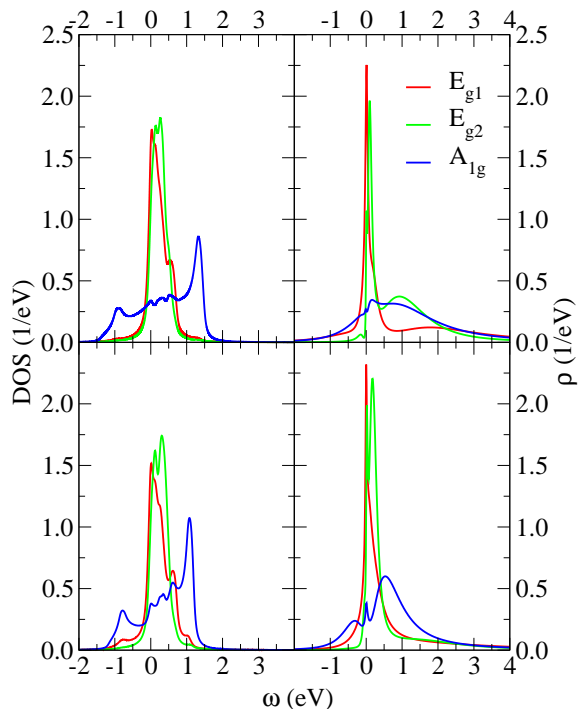


**Figure 7.** (Color online) Comparison of the LDA Wannier DOS (left) and local spectral functions from LDA+DMFT (right) for  $BaVS_3$  with  $U=3.5$  eV (top) and  $BaVSe_3$  with  $U=2.5$  eV (bottom).

Figure 7 shows the density of states derived from the original Wannier functions compared to the local spectral functions from DMFT for both systems. On the LDA level, the plot shows the reduced bandwidth of the selenide compound, with the orbital resolved effective widths within the  $t_{2g}$  manifold becoming more similar. Furthermore the overall stronger hybridization (note the use of the crystal-field basis) between  $A_{1g}$  and  $E_{g1}$  in  $BaVSe_3$  is clearly visible. This leads also to a more pronounced  $A_{1g}$  quasiparticle peak right at the Fermi level in the DMFT local spectral function.

As explained in [32, 12], the importance of explicit many-body effects in deforming the LDA Fermi surface appears as a crucial ingredient for the onset of the CDW in  $BaVS_3$ . Therefore, figure 8 shows the DMFT(CTQMC) quasiparticle Fermi surfaces for both chalcogenides. Correspondingly, figure 9 displays the quasiparticle dispersion for the closed path in the first BZ connecting the points 'M/2' and 'A/2' (see figure 2), which mark the relevant distance for the possible CDW nesting. The plots render it obvious that no definite information about the absence of the CDW in  $BaVSe_3$  can be retrieved from this viewpoint. Since qualitatively the same charge-transfer mechanism applies to the selenide compound, it may be observed that also the FS deformations go in the same direction. This means that within the LDA+DMFT accuracy also for smaller Hubbard  $U$  the experimental nesting condition could in principle be realized in  $BaVSe_3$ . Note however that in the selenide for  $U=2.5$  eV the respective quasi-1D sheets are still not strongly flattened.

In order to get a quantitative comparative understanding of the degree of quasi-

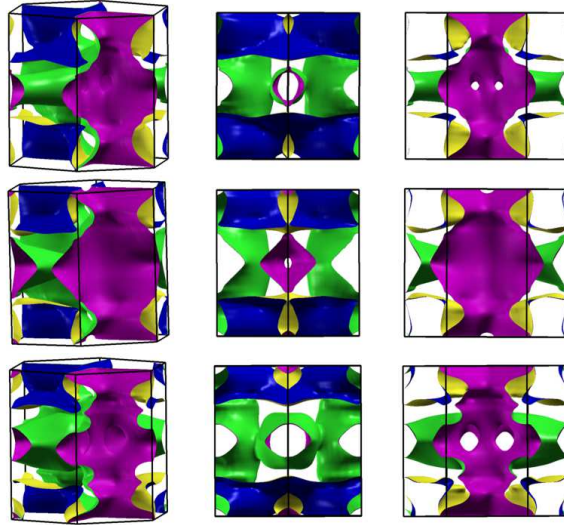


**Figure 8.** (Color online) Quasiparticle Fermi surfaces of  $BaVS_3$  with  $U=3.5$  eV (top) and  $BaVSe_3$  with  $U=3.5$  eV (middle) and  $U=2.5$  eV (bottom).

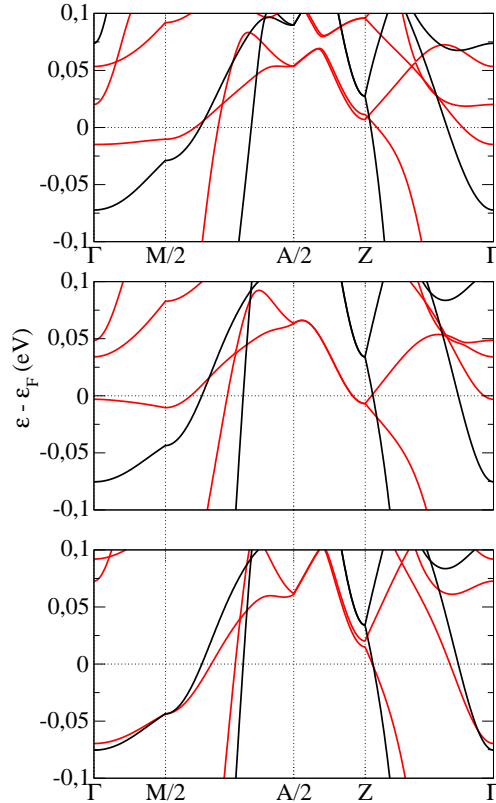


**Figure 9.** (Color online) Effective  $t_{2g}$  Wannier band structure with (red/grey) and without (black/dark) renormalization from LDA+DMFT along the closed path including 'M/2' and 'A/2' (see figure 2) for  $BaVS_3$  (top) and  $BaVSe_3$  with  $U=3.5$  eV (middle) and  $U=2.5$  eV (bottom).

onedimensionality of the two materials, we investigated the theoretical order of magnitude of the anisotropy in the DC conductivities in LDA as well as in the strongly

**Table 2.** Relation of the spatial components of squared Fermi velocities in  $BaVS_3$  and  $BaVSe_3$  on the LDA level and within LDA+DMFT(CTQMC) for a given  $U$  (in eV).

ratio	$BaVS_3$		$BaVSe_3$		
	LDA	$U=3.5$	LDA	$U=2.5$	$U=3.5$
$\langle v_z^2 \rangle / \langle v_x^2 \rangle$	3.7	2.7	4.8	5.2	3.0
$\langle v_z^2 \rangle / \langle v_y^2 \rangle$	8.3	9.9	10.7	9.9	10.2

correlated case. To this, table 2 summarizes the relation of the spatial components of the averaged Fermi velocities squared ( $\langle \mathbf{v}_F^2 \rangle = \langle v_x^2 \rangle + \langle v_y^2 \rangle + \langle v_z^2 \rangle$ ), whereas  $y$  denotes the spatial direction in which the zig-zag distortion of the vanadium chains can be observed. Note that the LDA values obtained for the sulfide are in perfect agreement with the elder result from Mattheiss [33]. Surprisingly, the selenide shows an even larger formal DC anisotropy in LDA compared to the sulfide compound. On the contrary it is also obvious that within the many-body approach of LDA+DMFT the renormalization of the anisotropy, especially in the dominant  $\langle v_z^2 \rangle / \langle v_x^2 \rangle$  channel leads to a balanced value for  $BaVSe_3$  with reasonable  $U=2.5$  eV. On the contrary, the quasiparticles become indeed significantly heavier in the  $c$  direction for  $BaVS_3$  with  $U=3.5$ . It is therefore worthwhile and interesting to note that the sulfide compound indeed displays a clear signature of DC anisotropy in the correlated case, whereas such a clear character is appearing in the according  $BaVSe_3$  data only at improper large  $U$ . It shall be remarked that the intraorbital quasiparticle weight for  $BaVS_3$  ( $BaVSe_3$ ) amounts to  $Z \sim 0.5$  (0.6) with minor differences within the  $t_{2g}$  manifold. Note that although we work in the crystal-field basis with a diagonal onsite KS hamiltonian for each of the two V atoms in the unit cell, the interacting terms together with the hybridization between those atoms lead to additional offdiagonal (interorbital) self-energy terms between  $A_{1g}$  and  $E_{g1}$  for the present crystal symmetry. Both many-body approaches, i.e. DMFT(CTQMC) and RISB, are capable of revealing and handling this effect. Thus a diagonal Green's function approach is invalid in the present case.

Finally, since the spin degree of freedom plays an additional vital role in these chalcogenide compounds, figure 10 exhibits the respective on-site spin-correlation functions from the LDA+RISB computations for constant ratio  $U/J=5$ . Concerning the diagonal spin-spin expectation value, as expected, the magnitudes evolve according to the nominal orbital occupations. Hence  $\langle S^2 \rangle$  for the effective  $E_{g1}$  orbital dominates over the corresponding value for the effective  $A_{1g}$  orbital in the strong-interaction limit. In this respect, again quantitatively  $BaVSe_3$  exceeds  $BaVS_3$  due to the increased  $E_{g1}$  occupation. The total  $\langle S^2 \rangle$  increases with larger  $U$  due to the growing electron localization. Note that in the present problem the magnitude of this diagonal quantity can exceed the atomic-limit value of a single electron, i.e.,  $\langle S^2 \rangle_{at} = \frac{1}{2}(\frac{1}{2} + 1) = \frac{3}{4}$ , albeit we have nominally one electron in the  $3d$  shell of the chalcogenides. This is due to the fact that at some point a strong Hund's coupling may tolerate an occupation of two electrons in the local three-orbital manifold of a metal. Since two electrons with parallel

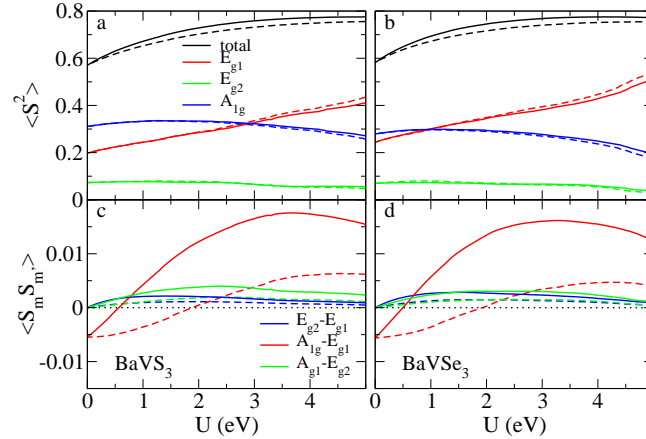


**Figure 10.** (Color online) On-site spin correlations for  $BaVS_3$  (left) and  $BaVSe_3$  (right). Dashed lines: density-density only interactions, solid lines: including also spin-flip and pair-hopping terms. In each  $U$  scan a ratio  $U/J=5$  was chosen. (a-b): Total and orbital-resolved diagonal spin-spin expectation value. (c-d): Off diagonal spin-spin correlation between the effective  $t_{2g}$  orbitals.

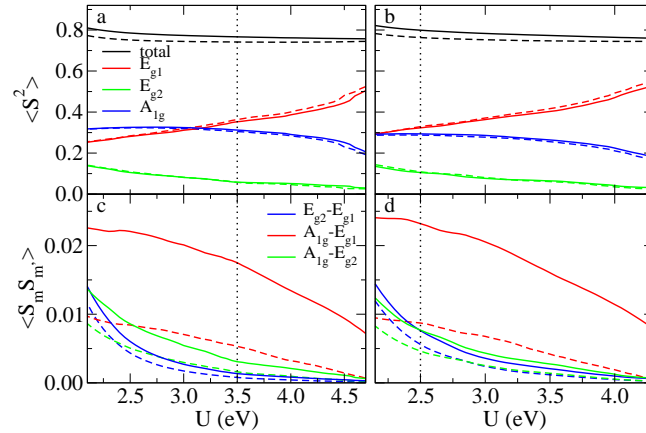


**Figure 11.** (Color online) Same as figure 10, but with fixed Hund's coupling  $J=0.7$  eV. The vertical dotted lines indicate the expected suitable choice for the Hubbard  $U$  of the respective system.

spin alignment form an  $S=1$  system, the resulting  $\langle S^2 \rangle$  is bigger than the sum of two individual single-electron occupied sites. The interorbital spin-spin correlations again prove the dominant  $A_{1g}-E_{g1}$  hybridization which leads also to a significant spin coupling. However it may be observed that in the minimal modeling for both systems the first Hund's rule is violated close to the  $U=0$ , i.e., the offdiagonal  $\langle S_{A_{1g}} S_{E_{g1}} \rangle$  becomes smaller than zero in this regime.

It also has to be noted that these interorbital spin-spin correlations are rather sensitive to the degree of approximation of the rotational invariance in the interaction. While the diagonal spin-spin expectation value is not strongly affected by the inclusion of spin-flip and pair-hopping terms in the local hamiltonian, the offdiagonal  $\langle S_m S_{m'} \rangle$  is strongly enhanced in this case by a factor of two to three. Thus whereas integrated one-

particle quantities like occupation numbers and local spins do not strongly suffer from density-density only descriptions, the two-particle functions, i.e., susceptibilities may be substantially different. Figure 11 displays the same spin-spin functions, but for the (more realistic) case of a constant  $J=0.7$  eV. Of course, the strongest response may be observed for smaller  $U$  since then the Hund's coupling is most effective. Note again the differences for the density-density only interactions, leading to an even qualitatively different behavior for small  $U$ , where  $\langle S_{A_{1g}} S_{E_{g1}} \rangle$  is eventually dominated by the  $\langle S_{E_{g2}} S_{E_{g1}} \rangle$ . In the more sound close-to rotational invariant description however,  $\langle S_{A_{1g}} S_{E_{g1}} \rangle$  is always clearly strongest. Because of the supposingly different  $U/J$  ratio for  $BaVS_3$  and  $BaVSe_3$  we hence expect for the selenide compound a more distinct magnetic behavior.

#### 4. Discussion

From the above calculations, it turns out that  $BaVS_3$  and  $BaVSe_3$  are in many respects very similar materials. The differences between them are rather subtle, but still large enough to be resolved by the applied methods. The picture that arises thereof is not totally unambiguous, but several hints can be given why the formation of a charge-density wave is hindered in  $BaVSe_3$ . Already on an LDA level, it can be seen that hybridization effects among the bands of the  $t_{2g}$  multiplet as well as with the corresponding S( $3p$ )/Se( $4p$ ) electrons, are significantly stronger in the selenide than in the sulfide. Hence a manifest discrimination between dominant  $A_{1g}$  and dominant  $E_{g1}$  character is far less obvious than in  $BaVS_3$ . Furthermore, the strong role of the effective  $A_{1g}$  orbital is weakened already on the LDA level and the final dominance of the effective  $E_{g1}$  orbital in the correlated case is even enhanced. This is altogether underlined by the DC anisotropies for the selenide, that under the effect of the expected correlations do not show the highlighting renormalizations in the  $c$  direction. Thus although the orbital differences are obvious, it seems as if the  $t_{2g}$  manifold in  $BaVSe_3$  acts somewhat more cooperatively compared to the largely competing scenario in  $BaVS_3$ .

With a surely smaller Hubbard  $U$  the selenide compound should also be closer to the LDA limit [14] with a less pronounced nesting susceptibility towards the CDW state. However as described, from a pure Fermi-surface discussion no clear answer to this question may be conveyed. Nevertheless, electronic correlations are not irrelevant in  $BaVSe_3$  as they underline the dominance of the  $E_{g1}$  level and the eventual importance of magnetic correlations. These latter are again stronger in the selenide compared to the sulfide, at least from a local viewpoint. Further calculations of intersite spin-spin correlations should shed more light onto this.

In the end, the present study within standard LDA+DMFT is not in the definite position to clearly assign the different experimental facts of these suprisingly similar compounds from a theoretical perspective. However albeit the situation is very subtle, we believe to have shown several indications that may motivate to a certain extent why the present compounds behave so differently at lower temperatures. There seem to exist two main possible instabilities in these chalcogenides, namely the CDW one and

the (ferro)magnetic ordering instability. As the driving forces towards these broken-symmetry states compete, a tailored renormalization-group study could reveal the finally dominating instability channel for each compound. Hence it is expected that the minor differences revealed in the present investigation show up more evidently within a renormalized scaling scenario. Still it has to be appreciated that though not fully comprehensive, the LDA+DMFT method is nowadays on a level where it is feasible to reveal fine details between rather similar materials.

## Acknowledgments

We wish to thank S. Schuwalow and C. Piefke for many fruitful discussions concerning the technical aspects of the theoretical approach. Furthermore we are indebted to O. Parcollet and M. Ferrero for providing their CTQMC implementation as well as to A. Akrap and V. Ilakovac for illuminating insights into recent experimental results obtained for these chalcogenide systems. Computations have been performed at the Norddeutscher Verbund für Hoch- und Höchstleistungsrechnen (HLRN).

## References

- [1] S. Ogawa. *J. Appl. Phys.*, 50:2308, 1979.
- [2] P. Monceau, N. P. Ong, A. M. Portis, A. Meerschaut, and J. Rouxel. *Phys. Rev. Lett.*, 37:603, 1976.
- [3] T. Nishikawa, Y. Yasui, Y. Kobayashi, and M. Sato. *J. Phys. Soc. Jpn.*, 65:2543, 1996.
- [4] O. Massenet, J.J. Since, J. Mercier, M. Avignon, R. Buder, and V.D. Nguyen. *J. Phys. C: Solid State Physics*, 40:573, 1979.
- [5] K. Matsuhara, T. Wada, T. Nakamizo, H. Yamauchi, and S. Tanaka. *Phys. Rev. B*, 43:13118, 1991.
- [6] M. Nakamura, A. Sekiyama, H. Namatame, A. Fujimori, H. Yoshihara, T. Ohtani, A. Misu, and M. Takano. *Phys. Rev. B*, 49:16191, 1994.
- [7] T. Graf, D. Mandrus, J. M. Lawrence, J. D. Thompson, P. C. Canfield, S.-W. Cheong, and L. W. Rupp. *Phys. Rev. B*, 51:2037, 1995.
- [8] C. H. Booth, E. Figueroa, J. M. Lawrence, M. F. Hundley, and J. D. Thompson. *Phys. Rev. B*, 60:14852, 1999.
- [9] L. Forró, L. Gaál, H. Berger, P. Fazekas, K. Penc, H. Berger, I. Kézsmárki, and G. Mihály. *Phys. Rev. Lett.*, 85:1938, 2000.
- [10] M.-H. Whangbo, H.-J. Koo, D. Dai, and A. Villesuzanne. *J. of Solid State Chem.*, 165:345, 2002.
- [11] S. Fagot, P. Foury-Leylekian, S. Ravy, J.-P. Pouget, and H. Berger. *Phys. Rev. Lett.*, 90:196401, 2003.
- [12] F. Lechermann, S. Biermann, and A. Georges. *Phys. Rev. B*, 76:085101, 2007.
- [13] T. Inami, K. Ohwada, H. Kimura, M. Watanabe, Y. Noda, H. Nakamura, T. Yamasaki, M. Shiga, N. Ikeda, and Y. Murakami. *Phys. Rev. B*, 66:073108, 2002.
- [14] A. Akrap, V. Stevanović, M. Herak, M. Miljak, N. Barišić, H. Berger, and L. Forró. *Phys. Rev. B*, 78:235111, 2008.
- [15] F. Sayetat, M. Ghedira, J. Chenavas, and M. Marezio. *J. Phys. C: Solid State Physics*, 15:1627, 1982.
- [16] J. Kelber, A. H. Reis, A. T. Aldred, M. H. Mueller, O. Massenet, G. Depasquali, and G. Stucky. *J. Solid State Chem.*, 30:357, 1979.

- [17] H. Nakamura, T. Yamasaki, S. Giri, H. Imai, M. Shiga, K. Kojima, M. Nishi, and K. Kakurai and N. Metoki. *J. Phys. Soc. Jpn.*, 69:2763, 2000.
- [18] T. Yamasaki, S. Giri, H. Nakamura, and M. Shiga. *J. Phys. Soc. Jpn.*, 70:1768, 2001.
- [19] V. I. Anisimov, A. I. Poteryaev, M. A. Korotin, A. O. Anokhin, and G. Kotliar. *J. Phys.: Condens. Matter*, 9:7359, 1997.
- [20] A. I. Lichtenstein and M. I. Katsnelson. *Phys. Rev. B*, 57:6884, March 1998.
- [21] T. Li, P. Wölfle, and P. J. Hirschfeld. *Phys. Rev. B*, 40:6817, 1989.
- [22] F. Lechermann, A. Georges, G. Kotliar, and O. Parcollet. *Phys. Rev. B*, 76:155102, 2007.
- [23] B. Meyer, C. Elsässer, F. Lechermann, and M. Fähnle. *FORTRAN 90 Program for Mixed-Basis-Pseudopotential Calculations for Crystals*. Max-Planck-Institut für Metallforschung, Stuttgart, (unpublished).
- [24] N. Marzari and D. Vanderbilt. *Phys. Rev. B*, 56:12847, 1997.
- [25] I. Souza, N. Marzari, and D. Vanderbilt. *Phys. Rev. B*, 65:035109, 2001.
- [26] A. A. Mostofi, J. R. Yates, Y.-S. Lee, I. Souza, D. Vanderbilt, and N. Marzari. *Comput. Phys. Commun.*, 178:685, 2008.
- [27] F. Lechermann, A. Georges, A. Poteryaev, S. Biermann, M. Posternak, A. Yamasaki, and O.K. Andersen. *Phys. Rev. B*, 74:125120, 2006.
- [28] A. Georges, G. Kotliar, W. Krauth, and M. J. Rozenberg. *Rev. Mod. Phys.*, 68:13, 1996.
- [29] P. Werner, A. Comanac, L. de' Medici, M. Troyer, and A. J. Millis. *Phys. Rev. Lett.*, 97:076405, 2006.
- [30] G. Kotliar, S. Y. Savrasov, K. Haule, V. S. Oudovenko, O. Parcollet, and C. A. Marianetti. *Rev. Mod. Phys.*, 78:865, 2006.
- [31] M. Ghedira, M. Anne, J. Chenavas, M. Marezio, and F. Sayetat. *J. Phys. C: Solid State Physics*, 19:6489, 1986.
- [32] F. Lechermann, S. Biermann, and A. Georges. *Phys. Rev. Lett.*, 94:166402, 2005.
- [33] L. F. Mattheiss. *Solid State Comm.*, 93:791, 1995.